JACS
JOURNAL OF THE AMERICAN CHEMICAL SOCIETY
pubs.acs.org/JACS
Article

Direct Observation of Group-V Dopant Substitutional Defects in CdTe Single Crystals

Akira Nagaoka,* Koji Kimura, Artoni Kelvin R. Ang, Yasuhiro Takabayashi, Kenji Yoshino, Qingde Sun, Baoying Dou, Su-Huai Wei, Koichi Hayashi, and Kensuke Nishioka

Cite This: J. Am. Chem. Soc. 2023, 145, 9191−9197
Read Online
ACCESS | Metrics & More | Article Recommendations | Supporting Information

ABSTRACT: Point defect chemistry strongly affects the fundamental properties of materials and has a decisive impact on device performance. The Group-V dopant is prominent acceptor species with high hole concentration in CdTe; however, its local atomic structure is still not clear owing to difficulties in definitive measurements and discrepancies between experimental observations and theoretical models. Herein, we report on direct observation of the local structure for the As dopant in CdTe single crystals by the X-ray fluorescence holography (XFH) technique, which is a powerful tool to visualize three-dimensional atomic configurations around a specific element. The XFH result shows the As substituting on both Cd (As_{Cd}) and Te (As_{Te}) sites. Although As_{Te} has been well known as a shallow acceptor, As_{Cd} has not attracted much attention and been discussed so far. Our results provide new insights into point defects by expanding the experimental XFH study in combination with theoretical first-principles studies in II−VI semiconductors.

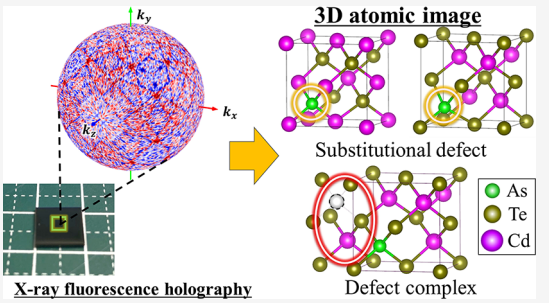

INTRODUCTION

Point defects often play a decisive role in the fundamental properties in the fields of physics and chemistry. In particular, the external substitutional defect due to the doping technology is essential for various semiconductor-based devices. Understanding the impact of a doping technique on functional-material properties is a fundamental challenge in semiconductors. However, experimental defect identification is typically difficult and indirect, usually requiring an ingenious combination of different techniques, which is still a significant issue for the development of semiconductors.

Doping is one of the promising approaches to achieve high carrier concentrations >10^{16} cm^{-3} by overcoming the doping limits of II−VI compounds.[1−10] At present, the strategy of group-V (P, As, Sb) doping, which is substituted at the Te site (e.g., P_{Te}, As_{Te}, Sb_{Te}), paves the way to high conversion efficiency >20% of CdTe-based photovoltaic (PV) devices.[2,3] Although many studies have been conducted over the last 50 years, detailed information on the defect structures of group-V doping is still not available, owing to difficulties in definitive measurements. The deleterious effects of defects on device performance can be avoided or mitigated only by clearly understanding the defect behavior.

The high doping activation efficiency (defined as hole concentration/total dopant concentration) has been an important aspect for semiconductor-based devices. The group-V doping activation in CdTe becomes less than 50% as doping is increased above ~10^{16} cm^{-3}, and the highest hole concentrations reported are in the low 10^{17} cm^{-3} range from experimental studies.[8,11−15] However, the origins of the doping limit, which may be caused by various mechanisms, have not been decisively established. We have experimentally observed secondary phase precipitates consistent with Cd_3As_2 along twin boundaries but only for samples with high As doping >10^{18} cm^{-3}, which indicates a solubility limit driven by the dopant chemical potential.[9,13] Theoretical calculations have suggested not only isolated point defects but also defect complexes.[4,8,16,17] Especially, a unique mechanism of self-compensation by metastable AX centers between shallow acceptor and donor-like asymmetric configurations with large lattice relaxation has been proposed which is still waiting for experimental confirmation. We have demonstrated metastable behavior through persistent photoconductivity-based measurements, which tend to support a local mechanism such as configuration switching of group-V dopant-related defects or clusters.[12,15] Additionally, thermodynamic and kinetic-based calculations of point defects, complexes, and reactions in As-doped CdTe reported that As interstitial (As_i)−As_{Te} and As_i−As_i defect complexes arise during activation annealing to form a kinetically stabilized transient state.[16]

Received: February 2, 2023
Published: April 17, 2023

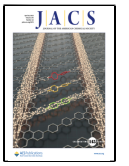

https://doi.org/10.1021/jacs.3c01248
J. Am. Chem. Soc. 2023, 145, 9191−9197

Table 1. Growth Conditions and As Doping Properties of CdTe Single Crystals

	Cd/Te	As doping concentration (cm^{-3})	doping activation (%)	annealing temperature (°C)	Cd vapor pressure (Pa)
sample A	1.01	6.5×10^{16}	24	750	9.5×10^{4}
sample B	1.05	8.5×10^{17}	30	950	6.9×10^{5}

So far, experimental studies on group-V dopant-related defects have relied on theoretical studies for discussing their results. This is because the direct observation of the three-dimensional (3D) structures of dopant arrangements has been difficult to achieve. X-ray absorption fine structure (XAFS) is a useful tool to provide structural information regarding dopants, but only with respect to the radial direction.[18−20] Atomic probe tomography (APT) analysis can be applied to the observation of the 3D dopant distribution in crystals, but several tens to several hundreds of nanoscale clustering of dopants is necessary.[21,22] In addition, high-resolution transmission electron microscopy (TEM)-based measurement has also been used to image individual dopants in real space and has provided data regarding the formation of dopant clusters,[21] but the atomic-resolution image has not been reported for this system. X-ray fluorescence holography (XFH) is a relatively new technique for local structural information of dopants, which can visualize 3D atomic configurations around a specific element without assuming any structural models.[23−25] Although the spatial resolution of XFH is worse than that of XAFS, XFH has a great advantage of 3D atomic images around the dopant within a wide range of about 1 nm.

In this study, we present the direct observation of group-V dopant-related substitutional defects in As-doped CdTe single crystals by XFH measurement. Local structural information of dopants in real space will provide the elucidation of the mechanisms of compensation for high group-V doping activation, which is one of the most important issues to achieve high performance of CdTe-based PV devices. In addition, reliable information on point defects resolves discrepancies between experimental observations and theoretical models in II−VI compounds.

EXPERIMENTAL SECTION

Sample Preparation. We grew high-quality As-doped CdTe single crystals with a Cd-rich composition using the traveling heater method.[26] Two types of bulk crystals (samples A and B) under Cd-rich conditions, summarized in Table 1, were grown for this study to identify the As-related defects. Grown crystals were cut into samples of approximately 5 mm × 5 mm × 1 mm with a diamond blade and polished mechanically with 0.1 μm Al_2O_3 paste and then etched with a 5% Br_2/methanol solution for 5 min to remove cutting and polishing damage. Ni-W Ohmic contacts of diameter 1 mm were deposited by RF sputtering onto the corners of each sample to a thickness of 200−300 nm for Hall effect measurement. Schottky diode structures of 1 mm diameter Al Schottky contact/CdTe (5 mm × 5 mm × 1 mm)/Ni-W Ohmic back contact were fabricated by evaporation onto each sample a thickness of 300−400 nm for admittance spectroscopy (AS) measurement. After contact fabrication, all samples were annealed at 250 °C in forming gas (96% N_2/4% H_2) for 10 min.

Physical and Structural Characterization. Hall effect measurements for hole concentration were carried out 300 K in a 0.45 T magnetic field in the van der Pauw geometry. I−V (current−voltage) sweeps on pairs of the Ni-W contacts indicated Ohmic behavior at all temperatures, and current and magnetic field reversals indicated good shape and contact resistance symmetry of the samples. AS measurements were carried out in the temperature range of 110−300 K under dark conditions with an LCR meter (HP 4284A), which applied an AC voltage of 50 mV by varying the frequencies from 50 Hz to 1 MHz. Photoluminescence (PL) was excited by a 10 mW power HeNe laser (632.8 nm) at 4 K. The dopant and impurity concentration in the grown crystals was determined by inductively coupled plasma atomic emission spectroscopy (ICP-AES). All dopant concentrations were nearly uniformly distributed over the entire ingot and wafer. Impurities such as Na, Cu, and Cl were measured less than 200 ppb. In addition, there are no observation of Cd_3As_2 secondary in all samples by infrared transmission microscopy. The XFH measurements were carried out at BL13XU in SPring-8, Japan. The As $K\alpha$ holograms (10.54 keV) of the samples A and B were measured by rotating the azimuthal (ϕ) and the polar (θ) angles in the ranges of $0° \le \phi \le 360°$ and $0° \le \theta \le 75°$, respectively. A cylindrical analyzer crystal was put between the sample and the avalanche photodiode detector to suppress the scattered X-rays and enhance the As $K\alpha$ fluorescent X-rays at the detecting position. The experimental setups are described in detail in ref 24. The energies of incident X-rays were set from 12.0 to 15.5 keV in steps of 0.5 keV, and thus totally eight holograms were recorded. From these holograms, the real-space image at position $\boldsymbol{r}$, $U(\boldsymbol{r})$, was reconstructed using Barton's method with the following equation,[24,27]

$$U(\boldsymbol{r}) = \int_k \mathrm{d}k \int_{|\boldsymbol{k}|=k} \chi(\boldsymbol{k}) Re\{\exp[i(k\boldsymbol{r} - \boldsymbol{k}\cdot\boldsymbol{r})]\}\mathrm{d}\boldsymbol{k} \quad (1)$$

where $\boldsymbol{k}$ is the wave vector and $\chi(\boldsymbol{k})$ is the holographic oscillation in the reciprocal space. Here, the integral $\int_k dk$ corresponds to the summation of the atomic images reconstructed from the holograms recorded with eight different incident X-ray energies.

Computational Method. Our first-principles calculations were performed by using the frozen-core projector augmented-wave (PAW) method[28] as implemented in the VASP code.[29] Since the local density approximation functional[30] severely underestimates the bandgaps of semiconductors, the Heyd−Scuseria−Ernzerhof (HSE06) hybrid functional[31] with $\alpha = 0.25$ is employed to correct the band gap of CdTe to 1.60 eV.[32] For the defect calculations, a $(2 \times 2 \times 2)$ supercell with 64 atoms is constructed, and the Γ-centered $(2 \times 2 \times 2)$ k-point mesh is used for Brillouin zone integration. The cutoff energy for plane wave basis is set to 350 eV. All the atoms in the supercell are fully relaxed until the Hellman−Feynman force on each atom is less than 0.02 eV/Å.

The defect formation energy as a function of the electron Fermi energy E_F and the atomic chemical potentials μ_i is given by[33]

$$\Delta H_f(\alpha, q) = \Delta E(\alpha, q) + \sum n_i\mu_i + qE_F \quad (2)$$

where $\Delta E(\alpha, q) = E(\alpha, q) - E(\text{host}) + \sum n_i E(i) + qE_{VBM}$. Here, $E(\alpha, q)$ is the total energy of a supercell with a defect α in charge state q, and $E(\text{host})$ is the total energy of the equivalent supercell without defects. q is the number of electrons transferred from the supercell to the Fermi reservoir in forming the defect cell. $E(i)$ is the total energy of constituent elemental i in its ground state solid or gas form, and $n_i$is the number of element i transferred to its chemical reservoir with chemical potentials $\mu_i$in forming the defect. E_F is the Fermi energy referenced to E_{VBM} which is the energy of the valence band maximum of the host. The defect transition energy level $\varepsilon_\alpha(q/q')$ is defined as the Fermi level at which defect α has the same formation energy in two different charge states q and q':

$$\varepsilon_\alpha(q/q') = [\Delta E(\alpha, q) - \Delta E(\alpha, q')]/(q' - q) \quad (3)$$

In addition, the binding energy[34] is defined as the difference between the lowest formation energy of the defect complex and corresponding isolated defects at the same Fermi level

$$E_b^q(E_F) = \Delta H_{f,\text{complex}}^q(E_F) - \sum_i \Delta H_{f,\text{defect}(i)}^q(E_F) \quad (4)$$

https://doi.org/10.1021/jacs.3c01248
J. Am. Chem. Soc. 2023, 145, 9191−9197

More negative binding energy indicates that it is easier to form the defect complexes when both isolated defects are present in the system.

Under the equilibrium growth condition, to have a stable CdTe compound, it should satisfy

$$\mu_{Cd} + \mu_{Te} = \Delta H_f(CdTe) = -1.19 \text{ eV} \quad (5)$$

To avoid the precipitation of the corresponding elemental solids and possible binary competitive phases, μ_i are bound by

$$\mu_i \leq =0 \quad (6)$$

$$m\mu_{Cd} + n\mu_{As} \leq \Delta H_f(Cd_mAs_n) \quad (7)$$

Here, Cd_3As_2 is taken as the limiting secondary phases because it is the most stable one in Cd_mAs_n compounds,[17] with a formation energy of −0.90 eV. Taking all the restrictions into consideration, the achievable chemical potential region is given in Figure S1.

RESULTS AND DISCUSSION

Fundamental Atomic Image by XFH. The hologram of the As *Kα* line in sample A is shown in Figure 1, which was measured at an incident energy of 12.0 keV. Obvious standing wave lines were observed in spite of low As concentration in sample A of 6.5×10^{16} cm^{-3}, showing that the experiments were successfully performed.

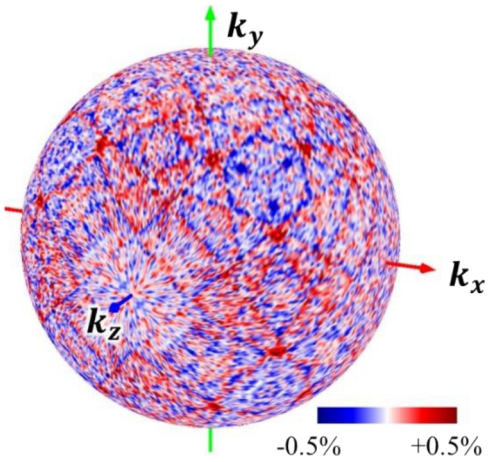

Figure 1. As *Kα* hologram obtained from sample A recorded at an incident X-ray energy of 12.0 keV.

The reconstructed atomic images of the plane situated at 1.6 Å above the As atom in samples A and B are shown in Figure 2a,b, respectively. We can observe clear atomic images within the solid circles, indicating the expected positions of Cd atoms around As_{Te} sites derived from the zincblende structure of CdTe (Figure 2c). This observation ascertains that As_{Te} substitutional acceptor defects are dominant in both samples A and B as the initial strategy of group-V doping. Moreover, it should be stressed that atomic images within thin-solid circles are observed in Figure 2a. Here, the thin circles correspond to the positions of the Te atoms around As atoms at the Cd sites (As_{Cd}: Figure 2d), and thus the presence of the As_{Cd} substitutional donor defect is indicated in sample A. On the other hand, the intensity of spots corresponding to As_{Cd} sites becomes much weaker for sample B in Figure 2b even though the As dopant concentration of sample B is 10 times higher than that of sample A. This observation shows the suppression of As_{Cd} donor defects by treatment of Cd vapor pressure of 6.9×10^5 Pa at 950 °C, which leads to higher doping activation. The reduction of the As_{Cd} donor defect leads to the reduction of self-compensation, which is consistent with the higher acceptor activation in sample B (30%) than that in sample A (24%). The self-compensation process in group-V doped CdTe has been proposed by the metastable AX center from previous theoretical studies; however, the AX configuration was not supported in this experimental XFH study. In a recent theoretical study on the supercell size and effects of spin-orbit coupling, the AX center was predicted to be unstable.[35] Moreover, Cd interstitial (Cd_i) under Cd-rich composition can be considered as a potential donor defect for self-compensation. The potential interstitial Cd_i and As_i defects and its related complexes were also not supported in this experimental XFH study.

Defect Properties. We attempted to reveal the further information of As_{Cd}-related defects on electrical properties. To understand the defect levels, we carried out the AS method based on capacitance measurements for both CdTe samples. Figure 3a,b shows the frequency-dependent capacitance spectra measured at different temperatures. Sample A shows a large variation in the low-frequency region compared with

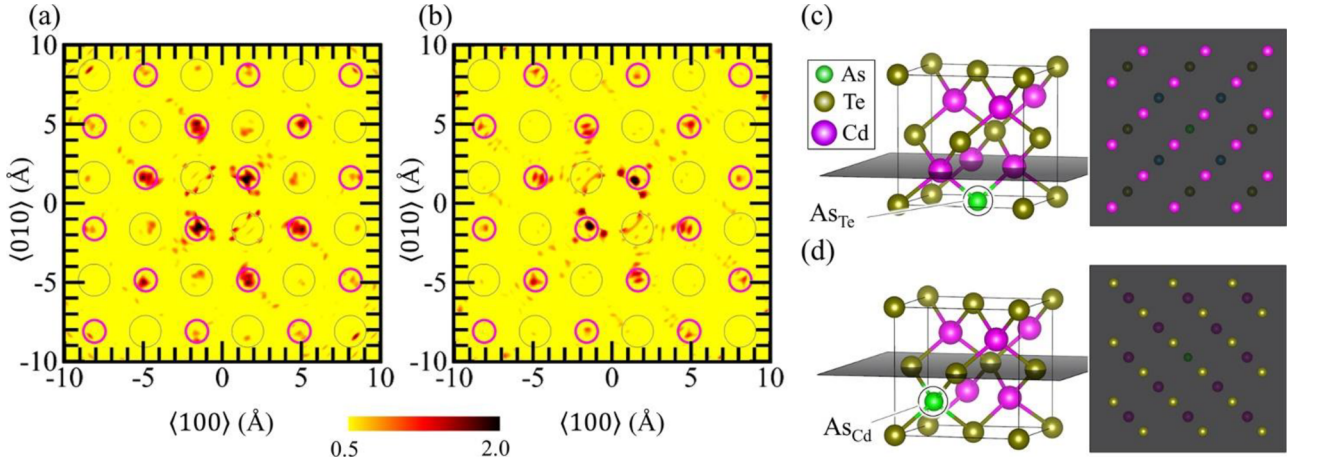

Figure 2. Reconstructed atomic images of the plane situated at 1.6 Å above the As atom in (a) sample A and (b) sample B, respectively. Solid and thin-solid circles indicate the expected positions of the Cd and Te atoms around the As_{Te} and As_{Cd} sites, respectively. (c, d) Schematic illustrations of the As_{Te} and As_{Cd} sites in the CdTe matrix crystal structure, where the Cd and Te planes ~1.6 Å above these As sites are also shown.

https://doi.org/10.1021/jacs.3c01248
J. Am. Chem. Soc. 2023, 145, 9191−9197

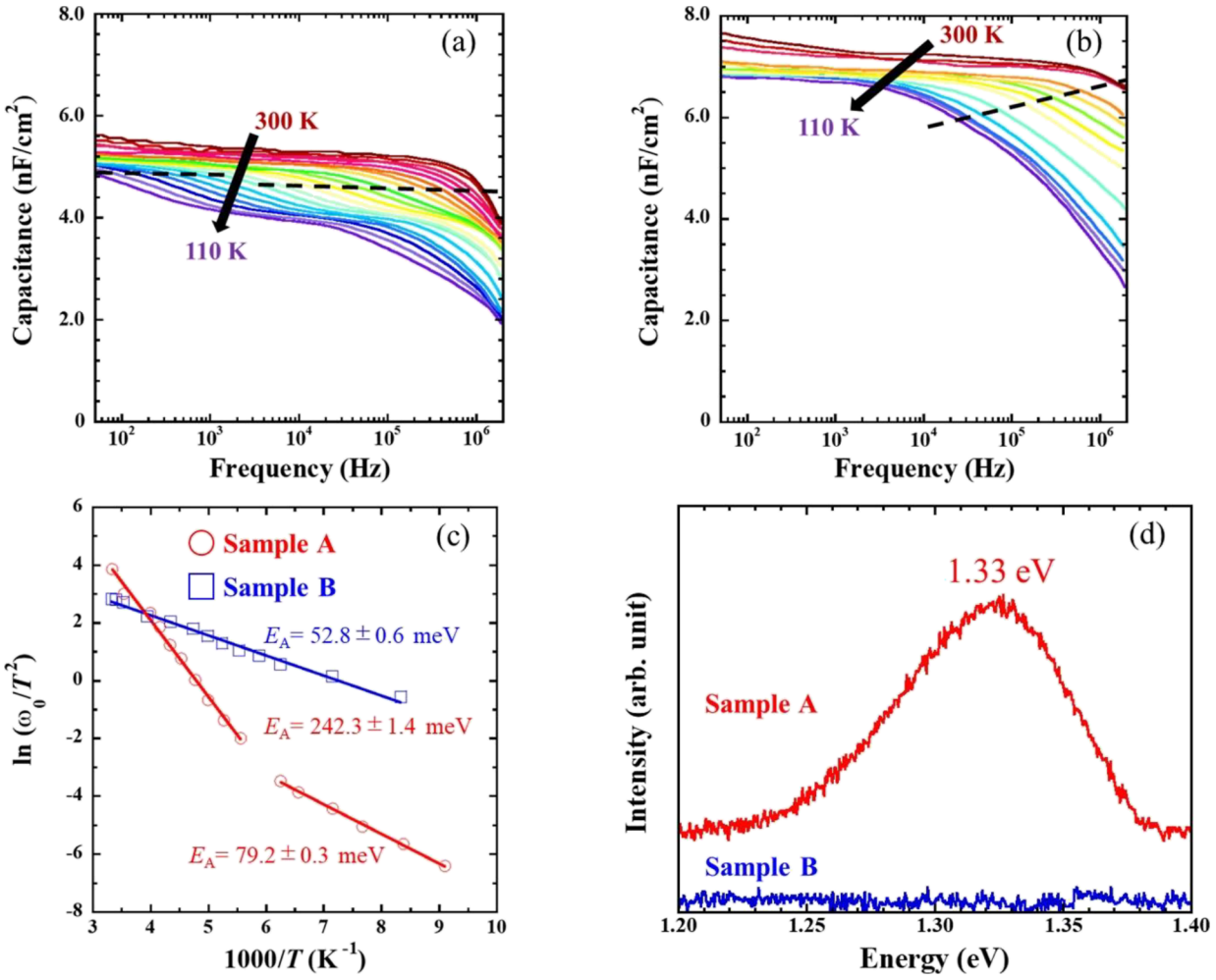

Figure 3. Admittance spectra (capacitance-frequency−temperature) of (a) sample A and (b) sample B, measured in the frequency range from 50 to 1 MHz at temperature from 110−300 K under dark conditions. Dashed lines mean the infection points of capacitance. (c) Arrhenius plots for sample A and sample B obtained from the infection points of the capacitance function. (d) PL emission spectra for both samples at 4 K, which the distinct peak at 1.33 eV can be observed in sample A.

sample B, which means the responses attributed to free carriers and deep defects whereas the capacitance at high frequency mostly represents the response due to free carrier concentration.[36] The capacitance steps are observable in both the spectra, and the inflection points were obtained from the maxima of the capacitance derivative. For verification the defect activation energy, we constructed an Arrhenius plot, shown in Figure 3c, of the inflection points from the AS curves. The Arrhenius plot was constructed using the following equation $\omega_0 = 2\pi\nu_0 T^2 \exp(-E_A/k_B T)$, where ω_0 is the infection point of the capacitance function, ν_0 is the pre-exponential factor, E_A is the defect level, and k_B is the Boltzmann constant.[37] The E_A values of both As-doped CdTe samples are very close for 50−70 meV, indicating the same origin of these defects. The shallow acceptor defects could be generally assigned as the dominant acceptor As_{Te} from our previous studies on temperature-dependent Hall effect measurement.[12,13] In addition, the emission of As_{Te} defects for both samples can be observed as the zero-phonon donor-acceptor pair (DAP) at 1.52−1.53 eV with 1LO to 3LO longitudinal optical phonon replicas[5,8] (Figure S2). Therefore, we revealed the 10−30 meV of the shallow donor level for As_{Cd} defects considering from the acceptor level of acceptor As_{Te} and bandgap of 1.60−1.61 eV for the CdTe material. Notably, the 240 meV of deep defect levels probably related to As_{Cd} in sample A can be detected. In addition, the distinct peak at 1.33 eV can be observed in sample A in Figure 3d, which is consistent with 240 meV of the deep defect level considering the bandgap of the CdTe material.

Next, we analyze the further information of deep acceptor level in sample A. The calculated atomic structures of isolated As_{Te} and As_{Cd} defects are shown in Figures 4 and S3. It is observed that the As_{Te} atom is located at an ideal position in Figure 4a, while the surrounding Cd atoms are shifted toward the As_{Te} atom, i.e., the As_{Te}−Cd bond length of 2.57 Å is shorter than the Te−Cd bond length of 2.81 Å. On the other hand, the As_{Cd}−Te bond length of 3.18 Å is largely shifted by approximately 0.6 Å in the ⟨111⟩ direction as shown in Figure 4b. Because totally three defect levels are indicated for sample A by the AS and PL measurements, another kind of defect should be considered. We focused on the Cd vacancy (V_{Cd}) defect which is important acceptor species having local distortion around Te atoms in CdTe.[38] It was reported that the V_{Cd} acceptor is induced by the As_{Cd} donor defect to form a V_{Cd}−As_{Cd} acceptor complex shown in Figures 4c and S3, which causes much less positional shift of the As_{Cd} atom in comparison with the simple As_{Cd} defect. The calculated formation energies of isolated defects (V_{Cd} and As_{Cd}) and

https://doi.org/10.1021/jacs.3c01248
J. Am. Chem. Soc. 2023, 145, 9191−9197

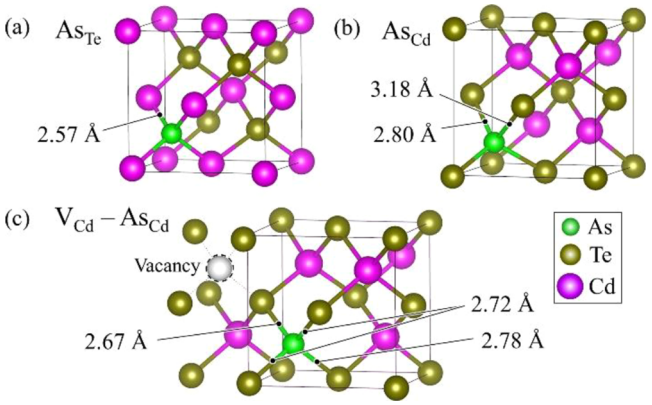

Figure 4. Atomic configurations of (a) As_{Te} and (b) As_{Cd} defects and (c) V_{Cd}–As_{Cd} defect complex derived from the first-principles calculations.

defect complex (V_{Cd}–As_{Cd}) are shown in Figure 5. The calculated results reveal that the As_{Cd} defect is a shallow single

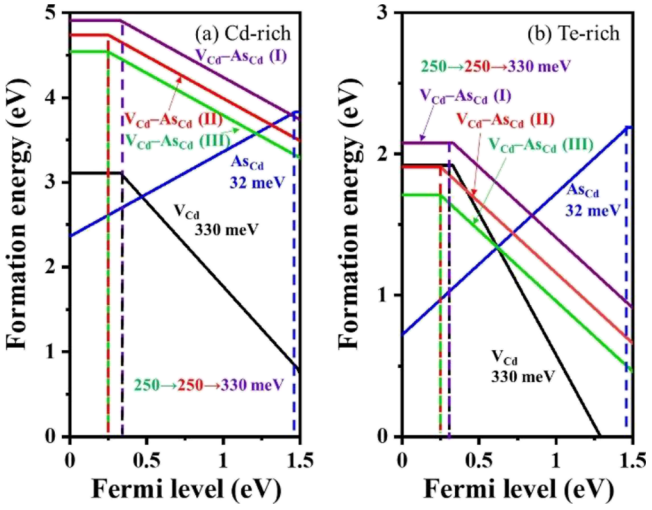

Figure 5. Calculated formation energies of isolated defects (V_{Cd} and As_{Cd}) and defect complex (V_{Cd}–As_{Cd}) as functions of the Fermi levels under (a) Cd-rich and (b) Te-rich conditions. The defect complexes with As_{Cd} at the first- (V_{Cd}–As_{Cd}(I)), second- (V_{Cd}–As_{Cd}(II)), and third- (V_{Cd}–As_{Cd}(III)) neighbor site of V_{Cd}.

donor with a transition level of 32 meV; however, the V_{Cd}–As_{Cd} complex is a deep single acceptor with transition levels varying from 250 to 330 meV when the As_{Cd} position changes from first- to third-neighbor site of V_{Cd} because of a level repulsion between the donor and acceptor levels. The level repulsion decreases when the distance between the two defects increases; thus, the acceptor complex level is deeper.

We simulated the atomic images of As_{Cd} and As_{Te} defects and V_{Cd}–As_{Cd} complex on the basis of theoretically derived atomic coordinates shown in Figure S4. The atomic image of sample A can be analyzed by the combination of simple substitutional As_{Cd} and As_{Te} defects and V_{Cd}–As_{Cd} complex in Figure 6, which is in good agreement with the experimental result in Figure 2a. From both experimental and theoretical results, we propose 30 meV of the As_{Cd} shallow donor and 240 meV of the V_{Cd}–As_{Cd} acceptor complex in sample A as low doping activation.

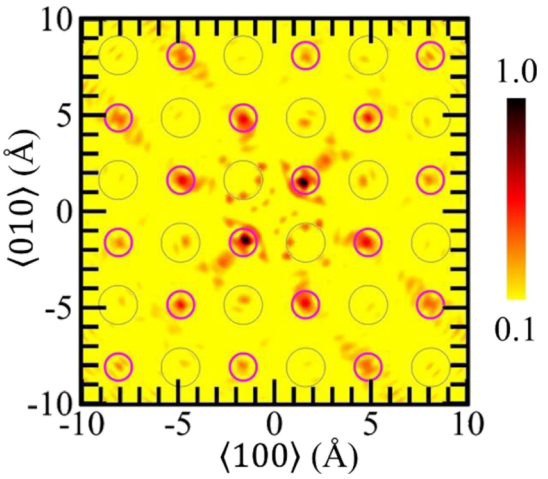

Figure 6. Simulated atomic image by the combination of simple substitutional As_{Cd} and As_{Te} defects and V_{Cd}–As_{Cd} complex for the experimental atomic image of sample A shown in Figure 1a.

CONCLUSIONS

In conclusion, the reliable local structure of group-V dopants in CdTe single crystals can be revealed by using XFH measurement as the direct observation method. As-dopants substituting at Cd and Te positions as As_{Cd} and As_{Te} defects can be experimentally observed under a Cd-rich composition, where As_{Cd} has not been discussed much in CdTe research community. We propose that As_{Cd} donor defects with 30 meV of shallow level dominate the self-compensation in As doped CdTe, which was assumed to be the AX center derived from early theoretical calculations in the field of II–VI semiconductors. The V_{Cd}–As_{Cd} defect complex level can be observed around 240 meV as evidenced by experimental measurements and theoretical calculations. These results inspire the importance of group-V dopant substitution on Cd sites in CdTe for both experimental and theoretical studies, which leads to higher efficiency in CdTe PV devices.

ASSOCIATED CONTENT

Supporting Information

The Supporting Information is available free of charge at https://pubs.acs.org/doi/10.1021/jacs.3c01248.

Figure S1, showing the chemical potential region for computational calculations; Figure S2, showing experimental defect levels in CdTe; and Figures S3 and S4, supporting experimental atomic images (PDF)

AUTHOR INFORMATION

Corresponding Author

Akira Nagaoka – *Research Center for Sustainable Energy & Environmental Engineering and Electrical and Electronic Engineering Program, University of Miyazaki, Miyazaki 889-2192, Japan;* orcid.org/0000-0003-3071-3899; Email: nagaoka.akira.m0@cc.miyazaki-u.ac.jp

Authors

Koji Kimura – *Department of Physical Science and Engineering, Nagoya Institute of Technology, Nagoya 466-8555, Japan;* orcid.org/0000-0001-5485-3672

Artoni Kelvin R. Ang – *Department of Physical Science and Engineering, Nagoya Institute of Technology, Nagoya 466-8555, Japan*

https://doi.org/10.1021/jacs.3c01248
J. Am. Chem. Soc. 2023, 145, 9191–9197

Yasuhiro Takabayashi − *Department of Physical Science and Engineering, Nagoya Institute of Technology, Nagoya 466-8555, Japan*
Kenji Yoshino − *Electrical and Electronic Engineering Program, University of Miyazaki, Miyazaki 889-2192, Japan*
Qingde Sun − *Beijing Computational Science Research Center, Beijing 100193, China; Hunan Provincial Key Laboratory of Flexible Electronic Materials Genome Engineering, School of Physics and Electronic Science, Changsha University of Science and Technology, Changsha 410114, China;* orcid.org/0000-0002-6216-4604
Baoying Dou − *Beijing Computational Science Research Center, Beijing 100193, China;* orcid.org/0000-0002-6797-2993
Su-Huai Wei − *Beijing Computational Science Research Center, Beijing 100193, China;* orcid.org/0000-0003-1563-4738
Koichi Hayashi − *Department of Physical Science and Engineering, Nagoya Institute of Technology, Nagoya 466-8555, Japan; Japan Synchrotron Radiation Research Institute (JASRI), Sayo, Hyogo 679-5198, Japan*
Kensuke Nishioka − *Research Center for Sustainable Energy & Environmental Engineering and Electrical and Electronic Engineering Program, University of Miyazaki, Miyazaki 889-2192, Japan*

Complete contact information is available at: https://pubs.acs.org/10.1021/jacs.3c01248

Notes

The authors declare no competing financial interest.

■ ACKNOWLEDGMENTS

A.N. acknowledges support from the JSPS KAKENHI Grant Number JP20K15221 and 2020 Young Researcher Award from Kenjiro Takayanagi Foundation. This work was also supported by the Japan Society for the Promotion of Science (JSPS) with Grants-in-Aid for Transformative Research Areas (A) "Hyper-Ordered Structures Science" (Nos. 20H05878 and 20H05881). The XFH experiment was performed at BL13XU of the SPring-8 with the approval of the Japan Synchrotron Radiation Research Institute (JASRI) (Proposals No. 2020A1207) and the authors thank Dr. Hiroo Tajiri for technical support. The work in China was supported by the National Natural Science Foundation of China (NSFC) (Grant Nos. 11991060, 12088101, and U2230402). We acknowledge the computational support from the Beijing Computational Science Research Center (CSRC).

■ REFERENCES

(1) Desnica, U. V. Doping limits in II−VI compounds — Challenges, problems and solutions. *Prog. Cryst. Growth Charact. Mater.* **1998**, *36*, 291−357.
(2) Burst, J. M.; Duenow, J. N.; Albin, D. S.; Colegrove, E.; Reese, M. O.; Aguiar, J. A.; Jiang, C. S.; Patel, M. K.; Al-Jassim, M. M.; Kuciauskas, D.; et al. CdTe solar cells with open-circuit voltage breaking the 1 V barrier. *Nat. Energy* **2016**, *1*, 16015.
(3) Metzger, W. K.; Grover, S.; Lu, D.; Colegrove, E.; Moseley, J.; Perkins, C. L.; Li, X.; Mallick, R.; Zhang, W.; Malik, R.; et al. Exceeding 20% efficiency with in situ group V doping in polycrystalline CdTe solar cells. *Nat. Energy* **2019**, *4*, 837−845.
(4) Yang, J.-H.; Yin, W.-J.; Park, J.-S.; Burst, J.; Metzger, W. K.; Gessert, T.; Barnes, T.; Wei, S.-H. Enhanced p-type dopability of P and As in CdTe using non-equilibrium thermal processing. *J. Appl. Phys.* **2015**, *118*, No. 025102.
(5) Burst, J. M.; Farrell, S. B.; Albin, D. S.; Colegrove, E.; Reese, M. O.; Duenow, J. N.; Kuciauskas, D.; Metzger, W. K. Carrier density and lifetime for different dopants in single-crystal and polycrystalline CdTe. *APL Mater.* **2016**, *4*, No. 116102.
(6) Colegrove, E.; Harvey, S. P.; Yang, J.-H.; Burst, J. M.; Albin, D. S.; Wei, S.-H.; Metzger, W. K. Phosphorus Diffusion Mechanisms and Deep Incorporation in Polycrystalline and Single-Crystalline CdTe. *Phys. Rev. Appl.* **2016**, *5*, No. 054014.
(7) Colegrove, E.; Yang, J. H.; Harvey, S. P.; Young, M. R.; Burst, J. M.; Duenow, J. N.; Albin, D. S.; Wei, S. H.; Metzger, W. K. Experimental and theoretical comparison of Sb, As, and P diffusion mechanisms and doping in CdTe. *J. Phys. D: Appl. Phys.* **2018**, *51*, No. 075102.
(8) Ablekim, T.; Swain, S. K.; Yin, W. J.; Zaunbrecher, K.; Burst, J.; Barnes, T. M.; Kuciauskas, D.; Wei, S. H.; Lynn, K. G. Self-compensation in arsenic doping of CdTe. *Sci. Rep.* **2017**, *7*, 4563.
(9) McCoy, J. J.; Swain, S. K.; Sieber, J. R.; Diercks, D. R.; Gorman, B. P.; Lynn, K. G. p-type doping efficiency in CdTe: Influence of second phase formation. *J. Appl. Phys.* **2018**, *123*, No. 161579.
(10) McCandless, B. E.; Buchanan, W. A.; Thompson, C. P.; Sriramagiri, G.; Lovelett, R. J.; Duenow, J.; Albin, D.; Jensen, S.; Colegrove, E.; Moseley, J.; Moutinho, H.; Harvey, S.; al-Jassim, M.; Metzger, W. K. Overcoming Carrier Concentration Limits in Polycrystalline CdTe Thin Films with In Situ Doping. *Sci. Rep.* **2018**, *8*, 14519.
(11) Yang, J.-H.; Yin, W.-J.; Park, J.-S.; Ma, J.; Wei, S.-H. Review on first-principles study of defect properties of CdTe as a solar cell absorber. *Semicond. Sci. Technol.* **2016**, *31*, No. 083002.
(12) Nagaoka, A.; Kuciauskas, D.; Scarpulla, M. A. Doping properties of cadmium-rich arsenic-doped CdTe single crystals: Evidence of metastable AX behavior. *Appl. Phys. Lett.* **2017**, *111*, No. 232103.
(13) Nagaoka, A.; Kuciauskas, D.; McCoy, J.; Scarpulla, M. A. High p-type doping, mobility, and photocarrier lifetime in arsenic-doped CdTe single crystals. *Appl. Phys. Lett.* **2018**, *112*, No. 192101.
(14) Nagaoka, A.; Nishioka, K.; Yoshino, K.; Kuciauskas, D.; Scarpulla, M. A. Arsenic doped Cd-rich CdTe: equilibrium doping limit and long lifetime for high open-circuit voltage solar cells greater than 900 mV. *Appl. Phys. Express* **2019**, *12*, No. 081002.
(15) Nagaoka, A.; Nishioka, K.; Yoshino, K.; Katsube, R.; Nose, Y.; Masuda, T.; Scarpulla, M. A. Comparison of Sb, As, and P doping in Cd-rich CdTe single crystals: Doping properties, persistent photoconductivity, and long-term stability. *Appl. Phys. Lett.* **2020**, *116*, No. 132102.
(16) Krasikov, D.; Sankin, I. Beyond thermodynamic defect models: A kinetic simulation of arsenic activation in CdTe. *Phys. Rev. Mater.* **2018**, *2*, No. 103803.
(17) Dou, B.; Sun, Q.; Wei, S.-H. Optimization of Doping CdTe with Group-V Elements: A First-Principles Study. *Phys. Rev. Appl.* **2021**, *15*, No. 054045.
(18) Espinosa, F. J.; Mustre de Leon, J.; Zapata-Torres, M.; Castro-Rodriguez, R.; Peña, J. L.; Conradson, S. D.; Hess, N. J. Direct observation of a lattice instability in heavily In-doped CdTe. *Phys. Rev. B* **1997**, *55*, 7629−7632.
(19) Espinosa, F. J.; Mustre de Leon, J.; Conradson, S. D.; Peña, J. L.; Zapata-Torres, M. Observation of a Photoinduced Lattice Relaxation in CdTe:In. *Phys. Rev. Lett.* **1999**, *83*, 3446−3449.
(20) Espinosa, F. J.; de Leon, J. M.; Conradson, S. D.; Peña, J. L.; Zapata-Torres, M. Local atomic structure of CdTe:In at high In concentrations. *Phys. Rev. B* **2000**, *61*, 7428−7432.
(21) Burton, G. L.; Diercks, D. R.; Ogedengbe, O. S.; Jayathilaka, P. A. R. D.; Edirisooriya, M.; Myers, T. H.; Zaunbrecher, K. N.; Moseley, J.; Barnes, T. M.; Gorman, B. P. Understanding arsenic incorporation in CdTe with atom probe tomography. *Sol. Energy Mater. Sol. Cells* **2018**, *182*, 68−75.
(22) Kartopu, G.; Oklobia, O.; Turkay, D.; Diercks, D. R.; Gorman, B. P.; Barrioz, V.; Campbell, S.; Major, J. D.; Al Turkestani, M. K.; Yerci, S.; et al. Study of thin film poly-crystalline CdTe solar cells

presenting high acceptor concentrations achieved by in-situ arsenic doping. *Sol. Energy Mater. Sol. Cells* **2019**, *194*, 259−267.
(23) Tegze, M.; Faigel, G. X-ray holography with atomic resolution. *Nature* **1996**, *380*, 49−51.
(24) Hayashi, K.; Happo, N.; Hosokawa, S.; Hu, W.; Matsushita, T. X-ray fluorescence holography. *J. Phys. Condens. Matter* **2012**, *24*, No. 093201.
(25) Ang, A. K. R.; Sato-Tomita, A.; Shibayama, N.; Umena, Y.; Happo, N.; Marumi, R.; Kimura, K.; Matsushita, T.; Akagi, K.; Sasaki, T.; et al. X-ray fluorescence holography for soft matter. *Jpn. J. Appl. Phys.* **2020**, *59*, No. 010505.
(26) Nagaoka, A.; Han, K.-B.; Misra, S.; Wilenski, T.; Sparks, T. D.; Scarpulla, M. A. Growth and characterization of Arsenic doped CdTe single crystals grown by Cd-solvent traveling-heater method. *J. Cryst. Growth* **2017**, *467*, 6−11.
(27) Barton, J. J. Removing multiple scattering and twin images from holographic images. *Phys. Rev. Lett.* **1991**, *67*, 3106−3109.
(28) Kresse, G.; Joubert, D. From ultrasoft pseudopotentials to the projector augmented-wave method. *Phys. Rev. B* **1999**, *59*, 1758−1775.
(29) Kresse, G.; Furthmuller, J. Efficient iterative schemes for ab initio total-energy calculations using a plane-wave basis set. *Phys. Rev. B* **1996**, *54*, 11169−11186.
(30) Perdew, J. P.; Levy, M. Physical Content of the Exact Kohn-Sham Orbital Energies: Band Gaps and Derivative Discontinuities. *Phys. Rev. Lett.* **1983**, *51*, 1884−1887.
(31) Paier, J.; Marsman, M.; Hummer, K.; Kresse, G.; Gerber, I. C.; Angyán, J. G. Screened hybrid density functionals applied to solids. *J. Chem. Phys.* **2006**, *124*, No. 154709.
(32) Madelung, O. *Semiconductors: Data Handbook*; Springer Science & Business Media, 2004.
(33) Wei, S.-H. Overcoming the doping bottleneck in semiconductors. *Comput. Mater. Sci.* **2004**, *30*, 337−348.
(34) Dou, B.; Sun, Q.; Wei, S.-H. Effects of co-doping in semiconductors: CdTe. *Phys. Rev. B* **2021**, *104*, No. 245202.
(35) Chatratin, I.; Dou, B.; Wei, S.-H.; Janotti, A. Doping Limits of Phosphorus, Arsenic, and Antimony in CdTe. *J. Phys. Chem. Lett.* **2023**, *14*, 273−278.
(36) Kimerling, L. C. Influence of deep traps on the measurement of free-carrier distributions in semiconductors by junction capacitance techniques. *J. Appl. Phys.* **1974**, *45*, 1839−1845.
(37) Walter, T.; Herberholz, R.; Müller, C.; Schock, H. W. Determination of defect distributions from admittance measurements and application to Cu(In,Ga)Se_2 based heterojunctions. *J. Appl. Phys.* **1996**, *80*, 4411−4420.
(38) Kavanagh, S. R.; Walsh, A.; Scanlon, D. O. Rapid Recombination by Cadmium Vacancies in CdTe. *ACS Energy Lett.* **2021**, *6*, 1392−1398.

https://doi.org/10.1021/jacs.3c01248
J. Am. Chem. Soc. 2023, 145, 9191−9197